

Nanoimprint Lithography and the Role of Viscoelasticity in the Generation of Residual Stress in Model Polystyrene Patterns**

By Yifu Ding, Hyun Wook Ro, Kyle J. Alvine, Brian C. Okerberg, Jing Zhou, Jack F. Douglas, Alamgir Karim, and Christopher L. Soles*

Understanding polymer deformation during the nanoimprinting process is key to achieving robust polymer nanostructures. Information regarding this process can be extracted from monitoring the decay of the imprinted polymer patterns during thermal annealing. In the present work, the effect of both the molar mass and the imprinting temperature on the pattern decay behavior during thermal annealing is investigated. Previously, it was found that the decay rate is fastest for a highly entangled polymer due to the elastic recovery caused by the residual stress created during the imprinting process. The present paper demonstrates that this residual stress level can be modified through control of the imprinting temperature. These results are contrasted with those for an unentangled polymer over a similar range of imprinting temperatures, where it is found that the pattern decay is controlled by simple Newtonian flow. In particular, the pattern decay is well described by surface-tension-driven viscous flow, and no imprinting-temperature effect is observed during thermal annealing. It is shown that the stability of the film against pattern decay can be optimized for moderately entangled polymer films. This effect is attributed to the competition between the effect of increased viscosity with increasing molar mass and increased residual stresses with entanglements. These observations provide guidance for the optimization of imprinting process in terms of selection of molar mass and processing temperatures.

1. Introduction

The contact printing of polymers using a hard mold is a rapidly developing technique with substantial promise.^[1–15] In addition to the potentially low fabrication costs and high throughput, this technique, known as nanoimprint lithography (NIL), can overcome the patterning resolution imposed by the diffraction limits in both traditional and immersion photolithographic methods. The features on the prepatterned mold can be replicated onto the resist materials via two different mechanisms: thermal embossing^[1–6,14,15] and UV-initiated crosslinking.^[7–15] Thermal-embossing NIL has

attracted broad interest because of its capability to directly pattern functional materials for various applications. Compared with indirect patterning of a resist, where subsequent additive and subtractive processes are required, this direct patterning can minimize the required number of processing steps. However, the stability of these “as-imprinted” structures then becomes a central concern in the development of this process.^[16,17]

Although low temperature patterning of glassy polymers has been demonstrated, most thermal-embossing NIL is performed at temperatures above the glass-transition temperature (T_g) of the polymer.^[18] The patterning resolution is determined by the viscoelastic deformation of thin polymer films under applied pressure. It is well known that the molar mass affects many of the physical properties of a polymer, especially rheological ones. The potential relevance of this variable for the NIL process both during and after pattern replication should thus be apparent. Specifically, a lower molar mass polymer having lower shear viscosity will tend to fill the mold more readily under given imprinting conditions.^[19] However, a larger molar mass polymer offers better cohesive strength, which is crucial for fabricating stable ultrasmall or high-aspect-ratio structures.^[20] Moreover, a relatively low molar mass polymer can also be more prone to dewetting from the substrate and/or the mold than higher molar mass polymers simply for kinetic reasons. Clearly, a proper selection of the polymer molar mass is important to optimizing the NIL process and achieving stable and faithful pattern replication.

[*] Dr. C. L. Soles, Dr. Y. Ding, Dr. H. W. Ro, Dr. K. J. Alvine, Dr. B. C. Okerberg, Dr. J. Zhou, Dr. J. F. Douglas, Dr. A. Karim, Polymers Division, National Institute of Standards and Technology, 100 Bureau Drive, Gaithersburg, Maryland 20899-8541 (USA)
E-mail: csoles@nist.gov

[**] This work is partially funded by the NIST Office of Microelectronic Programs. K. J. Alvine and B. C. Okerberg acknowledge the support of the National Research Council NIST Postdoctoral Fellowship Program. We acknowledge the nanofabrication laboratory of the Center for Nanoscale Science and Technology (CNST) at NIST for providing facilities for the nanoimprint process. This work is an official contribution of the National Institute of Standards and Technology; not subject to copyright in the United States. Certain commercial materials and equipment are identified in this paper in order to specify adequately the experimental procedure. In no case does such identification imply recommendation by the National Institute of Standards and Technology nor does it imply that the material or equipment identified is necessarily the best available for this purpose. The error bars presented throughout this manuscript indicate the relative standard uncertainty of the measurement.

The present investigation is a continuation of our previous studies on the stability of imprinted polymer patterns under different thermal annealing conditions.^[17] These works demonstrated that the pattern decay rate of highly entangled polystyrene (PS) is higher than that of the unentangled PS, despite the fact that the latter has a viscosity several orders of magnitude lower (and thus a higher mobility). This dramatic effect was attributed the fact that the imprint process induced significant residual stresses into patterns of the highly entangled PS.^[17] Here, we focus on the effect of the imprinting temperature on post-imprinted PS pattern stability for a range of molar masses by tracking the pattern height decay as a function of annealing time. The goal of our study is to determine the fundamentals of resist flow and process-induced residual stress from the analysis of a model polymer, PS.

2. Results and Discussion

2.1. Influence of Molar Mass on the Pattern Decay Rate

To study the pattern height evolution, atomic force microscopy (AFM) measurements were carried out on imprinted PS patterns annealed for different lengths of time. A series of PSs were used for the study, with molar masses of 18 700 g mol⁻¹, 96 900 g mol⁻¹, and 1 510 000 g mol⁻¹, referred to as PS_{xxk} from now on (for example, PS18.7k; see Experimental for details). Figure 1 shows the representative AFM images for PS18.7k patterns with 430 nm pitch before and after annealing for 146 min. For comparison, the cross-sectional scanning electron microscopy (SEM) images of the same samples are shown in the insets of Figure 1. The sharp corners of the as-imprinted pattern (inset of Fig. 1a) reflect the high fidelity of pattern replication from the mold. The pattern height measured by AFM is consistent with the SEM images (~360 nm, see Table 1), however the pattern widths cannot be precisely measured by AFM. Specifically, the trench widths in the AFM image (Fig. 1a) are narrower than those shown in the corresponding SEM image due to the AFM tip convolution. As the pattern height decays with annealing time, the tip tracks the

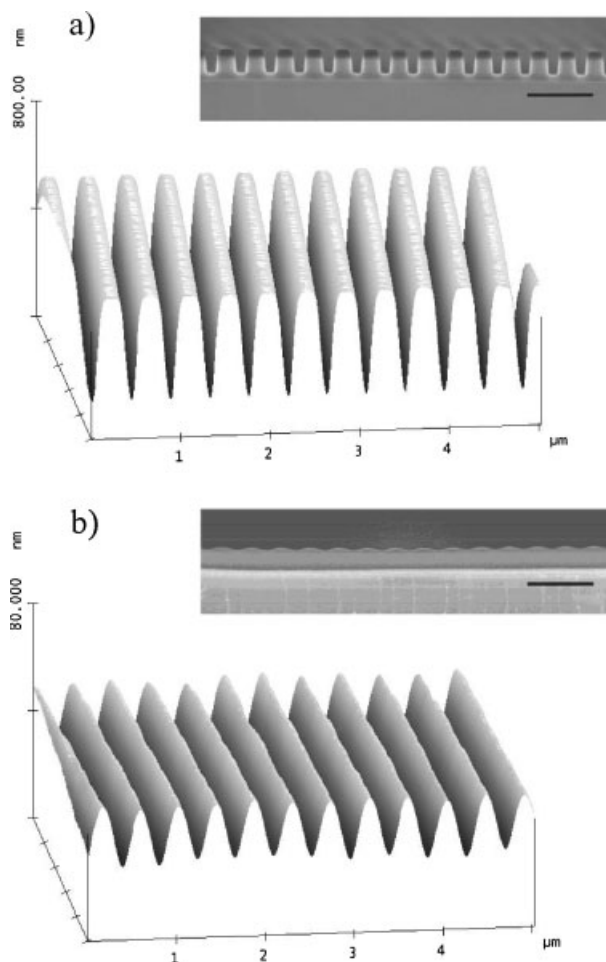


Figure 1. Representative three-dimensional rendering AFM topography of the PS18.7k patterns with 430 nm pitch a) as-imprinted and b) after annealing for 146 min at T_g . Note that the vertical scales for a) and b) differ by a factor of 10. The insets are the cross-sectional SEM images of the same samples. The scale bars in both SEM micrographs represent 1 μ m length.

profile of the patterns more effectively (Fig. 1b). Nevertheless, only the peak pattern height data from the AFM measurements is analyzed in the present study.

Figure 2 shows the pattern height as a function of annealing time at the T_g (see Table 1) of the corresponding PS for 430 and 850 nm pitch patterns imprinted at $T_g + 40^\circ\text{C}$. For each molar mass, the decay rate of the 430 nm pitch pattern is faster than the 850 nm pitch pattern, that is, the smaller patterns relax faster. For the patterns with the same pitch, 430 nm or 850 nm, the relative trend in the initial decay rate of different molar masses is: PS1510k > PS18.7k > PS96.9k. Consistent with our previous study,^[17] the highest molar mass PS shows the fastest pattern decay. The PS1510k also shows an interesting two-stage decay process that is not seen in the lower molar mass samples. Initially, the pattern height decays very quickly down to about 10% of its original height for 430 nm pitch

Table 1. KWW parameters (Eq. (5)) from fitting the pattern height decay in Fig. 4, and the effective viscosity estimated from Eq. (3). All values correspond to annealing temperature, not imprinting temperature.

M (kg mol ⁻¹)	R_g (nm)	T_g (°C)	T_{imp} (°C)	H_{Film} (nm)	PH (nm)	RL (nm)
18700	3.3	100	140	306.0 ± 2.3	362.1	88.8
			120	305.0 ± 0.7		
			180	304.9 ± 0.6		
96900	7.4	102	142	310.3 ± 0.7	366.2	91.8
			122	308.0 ± 1.2		
			182	307.4 ± 2.2		
1510000	29.3	106	146	313.1 ± 1.3	372.3	93.9
			126	313.9 ± 0.7		
			186	310.9 ± 1.1		

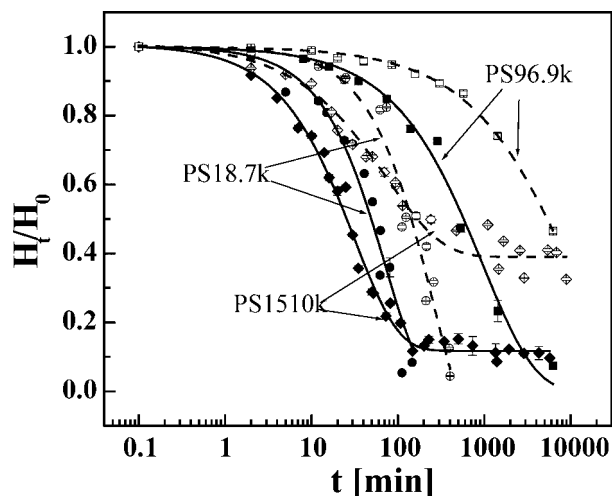


Figure 2. Pattern heights normalized by their initial value (as-imprinted, see Table 1), as a function of annealing time at T_g for both 430 nm pitch (solid symbols) and 850 nm pitch (empty symbols) patterns of the PS18.7k (circles), PS96.9k (square) and PS1510k (diamond), respectively. The lines represent fits to a stretched exponential decay: the solid lines correspond to the 430 nm pitch patterns, and dash lines correspond to the 850 nm pitch patterns.

pattern (40% for 850 nm pitch pattern), after which a plateau-like region occurs (after annealing after about 200 min for 430 nm pitch pattern and 600 min for 850 nm pitch pattern, see Fig. 2) and the decay rate drops significantly. For both PS18.7k and PS96.9k, no such plateau-like response was observed and the patterns entirely disappear within the experimental time (except for the 850 nm pitch pattern of PS96.9k due to the limited annealing time).

Our previous measurements of the decay kinetics of slightly smaller patterns found that the initial decay rate of highly entangled polymers indeed shows higher decay rates than unentangled ones, despite their several orders of magnitude higher viscosity.^[17] This fast decay of high-molar-mass patterns was attributed to the recovery of residual stresses, induced by the elastic deformation of the material during the imprinting process.^[17] It is intriguing that the medium-molar-mass PS shows the highest stability by merit of having the slowest pattern decay rate. In the following section, we show that the change in the pattern decay rates for different molar mass PS is determined by the differences in the underlying pattern decay mechanisms.

2.1.1. Pattern Decay Mechanism

In general, the relaxation of a surface pattern in a simple liquid is determined by the balance between the thermodynamic driving force and the kinetic resistance.^[21–23] The thermodynamic driving force for pattern decay is governed by the surface tension of the liquid (γ) and the surface curvature, whereas the apparent viscosity of the liquid (η) controls the rate. For patterned or rough liquid surface, the local curvature induces a Laplace pressure $P = \gamma/R$, where R indicates the local radius of curvature describing the surface pattern or roughness.

R tends to infinity for a smooth surface meaning that the Laplace pressure, and thus the surface free energy, is minimized. In the case of a polymer liquid, γ is a function of both molar mass of the polymer and the temperature. However, for relatively large molar mass PS ($M > 3000 \text{ g mol}^{-1}$), the variation in γ with changing molar mass is negligible at the same temperature ($\gamma \approx 0.033 \text{ N m}^{-1}$ at T_g).^[24] Given the molar masses of our PS, it is reasonable to assume that γ is constant for all. Moreover, the dimensions of the as-imprinted pattern are also identical for different molar mass PS patterns with the same pitch (see Experimental Section), meaning identical local curvature R and total excess surface area ($A_e = A_{\text{pattern}} - A_{\text{flat film}}$). The total excess surface energy ($E_e = E_{\text{pattern}} - E_{\text{flat film}} = \gamma A_e$) of patterns with the same pitch is therefore identical between different PS. This means that the surface tension component driving the pattern decay is similar for all 430 nm (or 850 nm) pitch patterns, regardless of the molar mass. Qualitatively, it is also clear that for the same molar mass PS, 430 nm pitch pattern should have larger driving force than the 850 nm pitch pattern during the annealing (see Fig. 2). Both the Laplace pressure and excess surface area (the pattern heights are similar between 430 nm and 850 nm) are larger for imprinted 430 nm pitch patterns. A quantitative analysis of the decay rate dependence on the pattern pitch will be presented below.

Since the thermodynamic driving force is identical for different PS patterns of the same pitch, the decay rate should be determined by η for the PS. Similar to γ , η also depends on temperature and PS molar mass.^[25,26] The mass dependence of η is especially large in highly entangled polymer melts. Specifically, in the limit of linear viscoelastic response, the steady state viscosity for unentangled polymers scales as, $\eta_0 \propto M^1$, where the molar mass $M < M_c$; M_c is the critical molar mass for entanglements $M_c \approx 38 \text{ kg mol}^{-1}$ for PS, and $\eta_0 \propto M^{3.4}$ in the highly entangled regime ($M > M_c$).^[25,26] In this study, the PS18.7k, PS96.9k and PS1510k fall into the categories of unentangled, moderately entangled and highly entangled, respectively. Over a wide temperature range above T_g , η_0 for PS can be estimated from the empirical Vogel–Fulcher–Tammann equation:

$$\eta_0 = A \exp\left(\frac{B}{\alpha_f(T - T_\infty)}\right) \quad (1)$$

where A is the structure factor that is a function of molar mass of PS; α_f is the expansion coefficient of the free volume; and the T_∞ is the Vogel temperature, at which the viscosity diverges to infinity. The values for A , B/α_f , and T_∞ can be found in Reference [28] for similar molar mass PS. Specifically, $B/\alpha_f = 1620 \text{ K}$ for all PS, $A = 5.90 \times 10^{-4} \text{ Pa} \cdot \text{s}$, and $T_\infty = 317 \text{ K}$ for the PS18.7k; $A = 2.67 \times 10^{-2} \text{ Pa} \cdot \text{s}$, and $T_\infty = 322 \text{ K}$ for the PS96.9k; For PS1510k, the viscosity is estimated through the viscosity-molar mass scaling shown above owing to the lack of experimental data. This means that the ratio of η_0 at the same temperature is roughly $1:50:6 \times 10^5$ for PS18.7k: PS96.9k: PS1510k

The amplitude or height of the pattern (H) decays exponentially with time t , with a rate governed by the surface tension and viscosity.^[22,23] For a linear grating having a sinusoidal cross section or line profile, the kinetics of the decay are described by^[22]

$$dH/dt = (-\pi\gamma H)/2\Gamma\eta \quad (2)$$

where Γ is the pitch of the grating. The corresponding exponential decay time (τ_d) is

$$\tau_d = \eta\Gamma/\pi\gamma \quad (3)$$

We note that the line profiles here are not exactly sinusoidal, especially at the early state of the annealing. The as-imprinted patterns have a rectangular-like profile (see Fig. 1a inset), which can be represented by a Fourier series

$$H(x) = \frac{4}{\pi} \sum_{k=1}^{\infty} \frac{\sin((2k-1)x)}{(2k-1)} \quad (4)$$

Roughly, three Fourier modes ($k=3$) can reasonably reproduce the rectangular-like line profile. During the annealing, the overall pattern profile evolution is a linear summation of its Fourier components of the line profile. Initially, the large Laplace pressure associated with the sharp corners of the as-imprinted PS patterns will round them off. Mathematically, this can be treated as a disappearance of high orders of the Fourier components. This process happens within a few min from the start of the annealing, without significant pattern height reduction, implying that Equations (2) and (3) are a reasonable approximation in this case.

In the steady state limit, the τ_d of the patterns with the same pitch and different molar mass mirror the molar mass dependence of η_0 , that is, the PS1510k patterns should decay at a rate five orders magnitude slower than the PS18.7k. Although the pattern decay is not necessarily dominated by the steady state flow, the reduced viscosity under similar stress (Laplace pressure)-induced shear thinning effect should still be orders of magnitude higher in the case of larger-molar-mass polymers.^[27,28] By contrast, Figure 2 shows that PS1510k has the fastest decay kinetics while the PS96.9k with an intermediate viscosity decays the slowest. Their differences in the pattern decay rates evidently cannot be understood within a simple model of surface tension driven viscous flow.

2.1.2. NIL Process

To understand the rheological aspects of the mold-filling process of the PS, Figure 3 presents both the segmental relaxation times (τ_α) associated with the glass transition and the chain relaxation times (τ_1 , which is the longest relaxation time of the polymer chain) of the three PS samples. At each imprinting temperature, τ_α is almost identical for all PS and several orders of magnitude shorter than the imprinting time ($\tau_{imp} = 180$ s). The chain relaxation time is estimated from

$\tau_1 \approx \eta_0 J_0$ where η_0 is estimated from the VFT equation parameters shown above and J_0 (steady state compliance) is obtained from Reference [28].

As shown in Figure 3, the τ_1 s of the PS18.7k and PS96.9k at 40 °C above their T_g (Table 1) are of the order of 0.01 s and 10 s, respectively, which is notably shorter than the imprinting time of 180 s. This suggests that imprinting-induced distortions of the polymer chains can be entirely relaxed during imprinting procedures for both polymers at this temperature; the molten polymer should behave like a Newtonian liquid during the imprinting, without significant elastic energy or residual stress stored in the replicated patterns. Upon annealing, these patterns should also decay according to the surface tension driven viscous flow mechanism. According to Equation (3), the decay time of the same pitch pattern will be determined by the viscosity of PS96.9k and PS18.7k. A quantitative analysis of the decay rate is presented below.

Shifting our attention to the highly entangled PS sample, Figure 3 shows that τ_1 of the PS1510k at T_g+40 °C is on the order of 10^5 s, a time significantly longer than the imprinting time. This suggests that entropic elasticity due to distortions of the entanglements and the stretching of the chain is still important.^[25,29] Since the applied pressure (3.4 MPa) is larger than the rubbery plateau modulus of the PS (approximately 0.2 MPa^[25]) at the imprint temperature, both elastic deformation of the quasi-network and viscous flow due to shear thinning of the melt are expected to contribute to the mold filling process. This results in a heterogeneous deformation inducing large amount of internal stress, which is not relaxed during the imprinting process ($\tau_1 \gg \tau_{imp}$, high Deborah number). When the system is cooled below T_g into the glassy state with the mold still in contact with the pattern, these stresses are frozen in or locked into the structure. When the PS1510k pattern is heated up to T_g , these residual stresses, in addition to the

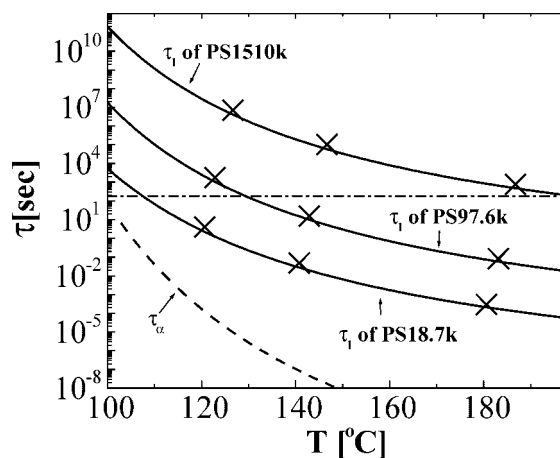


Figure 3. Temperature dependence of the bulk segmental relaxation time (τ_α , dash lines) and the chain relaxation (τ_1 , solid lines, see text for details) for the different molar mass of PS. The dot-dash line represents the time scale of the imprinting processes (180 s). The crosses mark the chain relaxation time of the PS at corresponding imprinting temperatures.

Laplace pressure, causes the PS1510k to decay at a much-accelerated rate relative to a model based on simple viscous flow and surface tension. In other words, elastic recovery is a major contributor to the pattern decay mechanism for PS1510k samples imprinted at this temperature. Following the initial elastic recovery, the pattern decay rate drops dramatically, exhibiting a slow plateau-like regime. This slow decay rate is typical behavior for the flow of highly entangled polymer melts.^[25] Presumably, if one waits long enough, an exponential decay of the pattern height can be found at very long time scales, with the decay time governed by Equation (3).^[17] However, at this annealing temperature the last stage is too slow to be observed experimentally, but can be observed by increasing the annealing temperature.^[17]

2.2. Effect of NIL Processing Temperature

As discussed above, NIL processing can induce relatively large amount of residual stress in the highly entangled PS1510k patterns, resulting from the disrupted network of the topological entanglements. If the imprinting time is much longer than the chain relaxation time, $\tau_1 \ll \tau_{imp}$, the residual stress can be fully relaxed. However, to achieve high throughput for the imprinting process, τ_{imp} is usually on the order of a few minutes or less. There is recent interest in roll-to-roll thermal imprint processes where imprint times would be substantially shorter and the mold would be separated from the roll at high temperatures.^[16] Under this circumstance, stress generation and pattern relaxation may be highly problematic for imprinting pattern stability. An alternative to extending τ_{imp} is to relax the imprint-induced stress is to raise the imprinting temperature (T_{imp}). As shown in Figure 3, the relaxation time, τ_1 decreases strongly with an increase of temperature, following the VFT equation, or equivalently, the Williams–Landau–Ferry (WLF) equation.^[25,26]

To explore the implication of this phenomenon further, we fabricated the patterns for the three different molar masses PS at 20 °C, 40 °C, and 80 °C above their respective T_g values (Table 1), with all other conditions kept the same (see Experimental Section). Figure 4 shows the time-dependent pattern height decay for these patterns annealed at T_g . For both 430 nm and 850 nm pitch patterns of PS18.7k (Fig. 4a), the pattern height showed very similar decay kinetics that only depended on the pattern pitch, for all values of T_{imp} . Figure 3 indicates that for PS18.7k at each T_{imp} , the condition that $\tau_1 \ll \tau_{imp}$ is always maintained. In these situations, the overall mold filling process is Newtonian-like. There is no difference observed between the thermal stability of these patterns fabricated at different imprint temperatures. Moderate imprinting temperature effects can be seen in the pattern decay response for PS96.9k (Fig. 4b). In Figure 3, it is evident that at 20 °C above T_g , the τ_1 of PS96.9k is about one order of magnitude longer than τ_{imp} , suggesting some residual stresses might exist in this case. At the two higher imprinting temperatures, the $\tau_1 \ll \tau_{imp}$ condition appears to be satisfied.

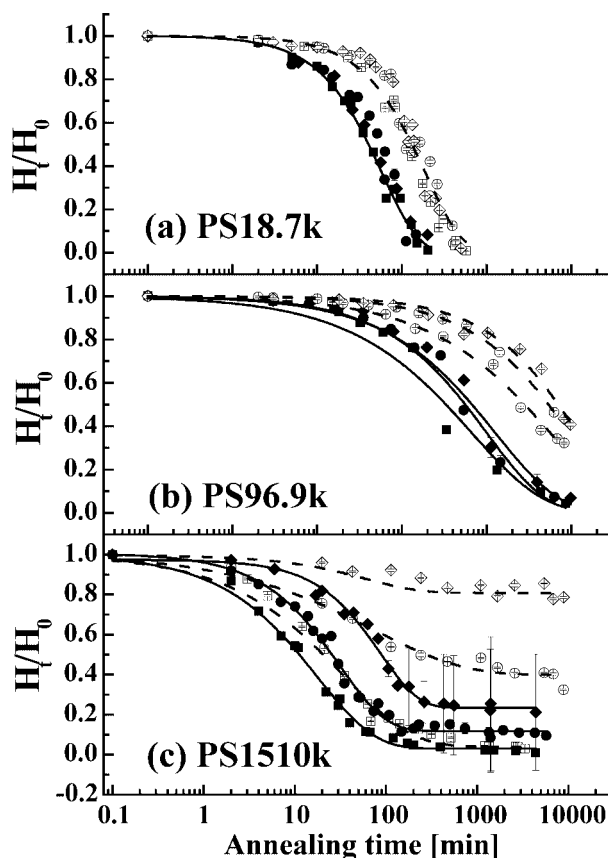


Figure 4. Normalized pattern height as a function of annealing time at T_g of the a) PS18.7k, b) PS96.9k, and c) PS1510k. The solid symbols represent 430 nm pitch patterns while the open symbols represent 850 nm pitch patterns. The different symbols represent the patterns imprinted at, $T_g + 20$ °C (square), $T_g + 40$ °C (circle), and 80 °C (diamond). The lines represent the stretched exponential fit of the experimental data (see text for details): solid and dashed lines correspond to the 430nm and 850nm pitch patterns, respectively.

We note that Figure 3 pertains to the zero-shear limit of viscous flow whereas the NIL molds are filled under much higher shear rates. The relatively weak influence of the imprinting temperature suggests that shear thinning instead of elastic deformation of rubbery network might be the main mold filling mechanism for PS96.9k. Consistent with this suggestion, no significant elastic recovery was observed during thermal annealing. The PS96.9k and PS18.7k pattern decay rates show weak or negligible dependence of the imprinting temperature and appear to be governed primarily by surface tension driven viscous flow. On the other hand, a significant dependence of the pattern decay on T_{imp} is observed in the case of PS1510k for both 430 nm and 850 nm pitch patterns, especially in the latter case. The level of the plateau-like region increases with T_{imp} , indicating the degree of elastic recovery decreases with the increase of imprint temperatures. Evidently, this pattern exhibits a “memory” of the processing history due to the viscoelastic nature of the entangled polymer melts.

To quantitatively describe the imprinting temperature effects, the pattern height decays in Fig. 4 were fitted

with a stretched exponential function, the Kohlrausch–Williams–Watts (KWW) equation, which is frequently used to parameterize the mechanical or dielectric relaxation of polymeric materials,^[30]

$$h_t = h_\infty + (1 - h_\infty) \exp(-(t/\tau)^\beta) \quad (5)$$

Here h_t and h_∞ are the pattern height (normalized by initial pattern height) after annealing for time t , and long time annealing ($t \rightarrow \infty$), respectively. β is the stretching exponent between 0 and 1.

The fitting curves are shown in Figure 4 with the fit parameters summarized in Table 2. Although the KWW equation is an empirical function, its parameters can give physical insight into the underlying relaxation process. Experimentally measured relaxational processes, such as the present case, are usually an ensemble average of many different local exponential relaxation processes. The stretching parameter β is normally interpreted as the relative breadth of the distribution of these relaxation processes. Broader distributions are reflected in smaller values of β , suggesting a more “stretched” relaxation process. The corresponding relaxation time (τ_{KWW}) determined from fitting Equation (5) is an average of the distribution of relaxation times.^[30]

In Figure 4, we see that the imprinted patterns of both the PS18.7k and PS96.9k (430 nm pitch) disappear within the experimental time scale, that is, h_t goes to 0. For PS18.7k, the fitting was performed collectively over the three different T_{imp} data sets. Figure 4a shows that both patterns (430 nm and 850 nm) of PS18.7k are reasonably described by a single exponential decay ($\beta = 1$), suggesting there is no significant distribution of the relaxation times. The small discrepancy between the fit and experimental data at very early decay times is probably due to the rounding of the sharp corners during the initial line height reduction; recall that the model here ignores the higher order Fourier components that would capture this corner rounding, especially during the early

stage of the annealing. In contrast, for both the PS96.9k and PS1510k patterns, the stretching parameter β is much smaller than 1, indicating the intrinsically heterogeneous distribution of local relaxation processes.

Table 2 also presents the effective viscosity (η_{eff}) of the PS estimated from the decay time (τ_{KWW}) for both 430 nm and 850 nm patterns, according to Equation (3). For PS18.7k, the value of η_{eff} estimated from the pattern decay rate is similar to η_0 , especially for the 850 nm pattern. However, the η_{eff} from 430 nm pattern imprinted at different temperatures for PS96.9k is about one order of magnitude lower than the η_0 , while η_{eff} approaches η_0 in the 850 nm patterns. This lower viscosity of 430 nm pitch pattern is probably a consequence of stress-induced shear thinning effect exerted in these patterns. In comparison to PS18.7k, the PS96.9k is more susceptible to the shear thinning, which is normal behavior for higher molar mass polymers.^[31,32]

For PS1510k, the τ_{KWW} increases only moderately with the imprinting temperature. As T_{imp} increases from $T_g + 20^\circ\text{C}$ to $T_g + 80^\circ\text{C}$, the average relaxation time, τ_{KWW} increases from approximately 18 min to 87 min for the 430 nm pitch pattern and 34 min to 61 min for the 850 nm pitch pattern. If τ_{KWW} is used to estimate η_{eff} from the viscous flow scenario, the resulting viscosities are about two orders of magnitude lower than that of the PS96.9k. The shear-thinning effect because of the Laplace pressure cannot account for such a dramatic reduction in PS1510k. Instead, elastic recovery is observed for the PS1510k. When T_{imp} increases, two effects come into play. First, the viscosity of the polymer decreases, which enhances the viscous flow during the mold-filling process. Correspondingly, the contribution from the elastic deformation of the entangled network decreases. Second, the terminal relaxation time decreases with temperature giving the distorted chains (and imposed stresses) more ability to relax in the duration of the imprint. Consequently, the percentage of elastic recovery in the pattern height decreases as the imprint temperature increases, from ~96% at $T_g + 20^\circ\text{C}$ to ~20% at $T_g + 80^\circ\text{C}$ in

Table 2. PS samples used for the NIL process and the dimensions of imprinted PS patterns measured by SXR. H_{film} is the initial film thickness before imprinting (measured by profilometry). PH is the initial pattern height and RL is the residual layer thickness measured by SXR. The uncertainty for PH and RL data is ± 1 nm.

		PS18.7k			PS96.9k			PS1510k		
		All T_{imp}	$T_g + 20^\circ\text{C}$	$T_g + 40^\circ\text{C}$	$T_g + 80^\circ\text{C}$	$T_g + 20^\circ\text{C}$	$T_g + 40^\circ\text{C}$	$T_g + 80^\circ\text{C}$		
430 nm Pattern	h_∞	0		0		0.02	0.12	0.23		
	τ_{KWW} (min)	58	669	1004	1209	18	31	87.1		
	β	1	0.52	0.62	0.68	0.67	0.86	1.04		
	η_{eff} (Pa · s)	9×10^8	1×10^{10}	1.6×10^{10}	1.9×10^{10}	2.8×10^8	4.8×10^8	1.4×10^9		
850 nm Pattern	h_∞	0		0		0.04	0.38	0.81		
	τ_{KWW} (min)	189	5665	9528	11866	34	50	61.4		
	β	1	0.52	0.64	0.69	0.58	0.31	0.76		
	η_{eff} (Pa · s)	2.9×10^9	8.8×10^{10}	1.5×10^{11}	1.8×10^{11}	5.3×10^8	7.8×10^8	9.5×10^8		
	η_0 (Pa · s)[b]	2.2×10^9		3.2×10^{11}			3.2×10^{15} [a]			

[a]Theoretical value. Practically, as the viscosity reaches 10^{13} Pa · s, the system is regarded as a glass. [b]Steady state viscosity of different PS at the annealing temperature estimated from the VFT equation.

the case of 850 nm patterns, and from $\sim 98\%$ at $T_g + 20^\circ\text{C}$ to $\sim 77\%$ at $T_g + 80^\circ\text{C}$ for the 430 nm patterns (see Table 2). After the rapid initial elastic recovery, the remaining patterns mainly decay through viscous flow, following Equation (3). Because of the high viscosity in the PS1510k patterns, this process is extremely slow. After long annealing times, the 430 nm pattern of PS1510k imprinted at $T_g + 80^\circ\text{C}$, begins to show signs of a lateral instability. The pattern uniformity starts to decrease, which leads to the large error bars for this data in Figure 4c. The nature of this lateral instability is the focus of a separate investigation.^[33]

To illustrate the feature-size effect on the decay rate, we consider the ratio of decay time between 850 nm and 430 nm patterns imprinted at different temperatures, as shown in Figure 5. Equation (3) indicates that the viscous flow time is proportional to the pattern pitch, indicates that 850 nm patterns should “melt” (structural disappearance) at nearly twice slowly as the 430 nm ones for the same PS. The ratios obtained from Figure 4 and Table 2 for PS18.7k are about three, which is close to the predicted ratio, and independent of the imprint temperature. Once again, this is nominally consistent with a simple surface tension and viscosity dependent pattern decay process. The ratio of PS1510k sample is also close to the prediction of Equation (3), except for the patterns imprinted at $T_g + 80^\circ\text{C}$ (Because of the instability in 430 nm pattern during annealing and the slight decay in 850 nm pattern, the uncertainty in this ratio is high.). This result indicates that mass transport due to the elastic recovery is similar to that for viscous flow, in that the process ultimately leads to a leveling of the surface patterns.

The most surprising observation is that the ratio (decay rate of 850 nm pattern to that of 430 nm pattern) for PS96.9k imprinted at all temperatures is much larger than two, although its pattern decay mechanism is primarily viscous flow, as discussed earlier. According to Mullins, several

mechanisms can contribute to the leveling of surface patterns.^[21] In the case of polymers, both viscous flow discussed above^[17,22,23] and surface diffusion^[34] processes have been reported as the surface leveling mechanism. Specifically, for surface diffusion mechanism, the decay time scales with pattern size as, $\tau_{\text{surface diffusion}} \sim \Gamma^4$,^[21,34] predicting the ratio between 850 nm and 430 nm patterns should be about 16. In general, viscous flow dominates the transport mechanism for large wavelength (pitch) patterns, while surface diffusion is more relevant for small wavelength (pitch) patterns.^[21,34] However, it is not clear at which threshold wavelength the mass transport mechanism changes from the viscous flow to surface diffusion in polymeric materials. Rafailovich et al. studied the decay process of thin PS films on top of shallow Si grating substrate, and they suggested that surface diffusion was the dominating mechanism of surface leveling.^[34] However, in our case, the large ratio between 850 nm and 430 nm pitch is more likely caused by a smaller effective viscosity in 430 nm pitch pattern because of the shear thinning (Table 2). In other words, both η_{eff} and Γ in Equation (3) are larger in 850 nm patterns, which causes this ratio deviates from the viscous flow predictions.

3. Conclusions

Thermal embossing NIL relies on the deformability of the polymers to achieve pattern replication. To faithfully replicate the features of the mold and obtain stable polymer patterns, an understanding of the deformation mechanisms during the processing is crucial. Here we focus on the influence of imprinting temperature on the stability of the imprinted patterns and on optimizing the molar mass for maximal stability of the imprinted patterns.

The measurements on highly entangled PS1510k suggest that significant amount of residual stress arises from the NIL process, which causes rapid pattern height decay during annealing. The level of residual stress (and resulting elastic recovery) can be mediated by raising the imprinting temperatures for PS1510k. For unentangled PS18.7k, the mold filling process is mostly Newtonian flow when imprinted from 20°C to 80°C above its T_g . Correspondingly, the pattern decay during the annealing is consistent with the surface tension driven viscous flow for two different pitch patterns. For moderately entangled PS96.9k, the pattern decay behavior suggests that the mold filling process was mostly a result of nonlinear flow when imprinted at 20°C above T_g , and Newtonian flow at 40°C to 80°C above T_g . The decay rate of the imprinted 850 nm patterns is close to the prediction of surface tension driven viscous flow. For smaller patterns (430 nm), the estimated effective viscosity is lower than the prediction, indicating the shear thinning effect. Overall, PS96.9k shows the most stable pattern during the annealing balanced by reducing the effect of elastic recovery (compared to PS1510k), while increasing the viscosity during annealing (compared to PS18.7k).

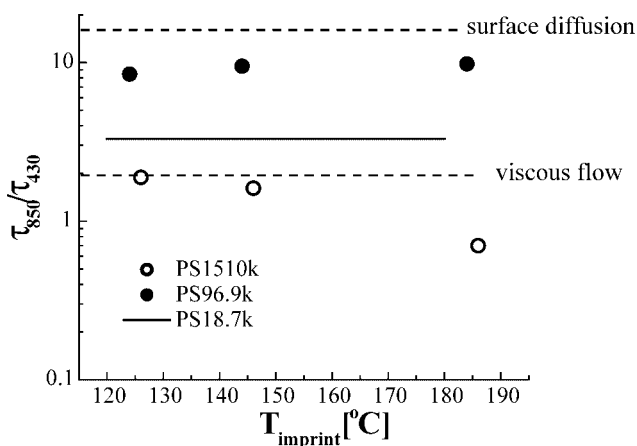


Figure 5. Ratio of the pattern decay rate between 850 nm and 430 nm pitch patterns imprinted at different temperature for PS18.7k (solid line), PS96.9k (filled circles) and PS1510k (open circles). Data from Table 2.

Attempts have been made to achieve high throughput in thermal embossing NIL, by directly demolding at high temperatures without the cooling process after the imprinting.^[16] Clearly, our study suggests that if high molar mass is utilized, significant reduction or lateral instability of the patterns might occur. Thermal “reflow” by heating the patterns above the T_g of the polymers to reduce the line-edge roughness also has been demonstrated by Chou et al. in the case of a commercial unentangled polymer resist.^[35] For highly entangled polymers, this process might cause significant pattern height change during “reflow”. Moreover, it is generally suggested that the imprint process should be carried out at lower temperatures, to minimize the thermal mismatch between polymer resist and substrate. In the case of highly entangled polymers, processing induced stress might also be an issue affecting the fabricated structures.

4. Experimental

A series of polystyrenes (PS) samples with different molar masses were purchased from Scientific Polymers, including PS18.7k, PS96.9k and PS1510k. The characterizations of the materials and as-imprinted structures are listed in Table 1. Thin films of PS were prepared by spin coating from a toluene solution onto silicon (Si) substrates. The Si wafers with a thin native oxide surface were treated in a UV-ozone cleaner (Jelight, Model No. 42) for 1 min to remove organic residues. The concentration (by mass) of the PS in the toluene was 6.7%, 5.1% and 2.4% for PS18.7k, PS96.9k and PS1510k, respectively. The spin coating was carried out at 209 rad s⁻¹ (2000 rpm) for 1 min. The as-cast films were annealed in a vacuum oven at 150 °C for 1 h to remove the residual solvent. Under these conditions, the thickness for all the samples, as measured by profilometry, was approximately 300 nm (Table 1).

The NIL processes were performed on a Nanonex NX-2000 tool. The imprinting mold consisted of parallel line-and-space gratings (with depth about 360nm) in silicon oxide with two different pitches, Γ , of about 430 nm and 850 nm, and each patterned area was 5 mm \times 20 mm. To facilitate the mold release after imprinting, a low surface energy fluorinated self-assembled monolayer was applied to the mold [36]. The films were first brought into contact with the mold at temperature below the T_g of the PS. The patterning processes were carried out under vacuum at a prescribed temperature above the bulk T_g of the PS and a pressure of 3.4 MPa for 3 min. The imprinted patterns with the mold in contact were cooled to 55 °C before releasing the pressure. Finally, the mold was separated from the PS patterns mechanically. For each molar mass PS films, imprints were performed at 20 °C, 40 °C, and 80 °C above the corresponding bulk T_g shown in Table 1.

Precise characterization of the fidelity of the pattern replication is not trivial. High-resolution metrologies for pattern shape characterizations are required. To meet this challenge, we are developing a set of X-ray based techniques, namely, critical-dimension small-angle X-ray scattering (CD-SAXS) [37–39] and specular X-ray reflectivity (SXR) [40,41]. By fitting the diffracted or specular reflected X-ray intensity, we can extract the dimensions of periodic patterns with nanometer resolution. A detailed description of the pattern shape characterization using SXR and CD-SAXS is given in References [39–43]. Here, we use SXR to characterize the initial fidelity of the pattern replication. For our line-space grating patterns, SXR measurements provide the pattern height, residual layer thickness (the remaining PS layer between the pattern and substrate), and line-space ratio as a function of the pattern height. The latter can be used to determine the absolute line width as a function of pattern

height with the pitch, provided by a CD-SAXS measurement, as a conversion factor. SXR measurements on both the patterned mold and imprinted PS structures show an excellent fidelity of pattern replication for all the different PS patterns imprinted at all the different temperatures. The PS sample information, including the initial film thickness before imprinting and the dimensions of the imprinted PS grating lines, are summarized in Table 1. We note that our residual layer thickness of the patterns (Table 1) are large enough to minimize the substrate effect.

To explore the pattern shape change with thermal annealing, Atomic Force Microscope (Dimension 3100, Veeco Instruments) was used to image the annealed PS patterns. Each imprinted pattern (5 mm \times 20 mm) on the Si substrate was sectioned into several smaller pieces (\approx 2 mm \times 5 mm). These pieces of the patterns were placed horizontally on a calibrated hot stage (Linkam, Model THMS600) with precise temperature control (Linkam, Model TMS94) and annealed at the bulk T_g of the corresponding PS for different amounts of time. Our previous studies have shown that the imprinting process does not cause notable change of T_g of the PS in these patterns [42]. The samples were then taken off the hot stage and cooled to room temperature in air. Two sets of experiments were carried out to verify the reproducibility of these AFM and annealing experiments.

It is known that a topographic AFM image of a surface is convoluted with the shape of the AFM tip. This difficulty becomes greater for small and closely packed structures with a high aspect ratio. To obtain faithful description of the pattern shape, special tips (such as flare tips) have to be used [16]. In this study, the purpose of AFM analysis is only limited to extracting the pattern height, not the full pattern profile. Special care was taken to ensure that AFM tips always touched the bottom of the trench between two adjacent lines to obtain an accurate measurement of the pattern height. The height measurements were calibrated with standard grating patterns with line height 400 nm. For 430 nm and 850 nm pitch patterns, 3 \times 3 μ m² and 5 \times 5 μ m² scans were performed, respectively. Uniformity of the pattern shape/height was confirmed by performing measurements at multiple spots on each sample.

Received: November 30, 2007

Revised: January 29, 2008

Published online: June 10, 2008

- [1] S. Y. Chou, P. R. Krauss, P. J. Renstrom, *Science* **1996**, 272, 85.
- [2] S. Y. Chou, P. R. Krauss, P. J. Renstrom, *Appl. Phys. Lett.* **1995**, 67, 3114.
- [3] S. Y. Chou, P. R. Krauss, P. J. Renstrom, *J. Vac. Sci. Technol. B* **1996**, 14, 4129.
- [4] M. D. Austin, H. X. Ge, W. Wu, M. T. Li, Z. N. Yu, D. Wasserman, S. A. Lyon, S. Y. Chou, *Appl. Phys. Lett.* **2004**, 84, 5299.
- [5] H. C. Scheer, H. Schulz, T. Hoffmann, C. M. S. Torres, *J. Vac. Sci. Technol. B* **1998**, 16, 3917.
- [6] G. L. W. Cross, B. S. O'Connell, H. O. Ozer, J. B. Pethica, *Nano Lett.* **2007**, 7, 357.
- [7] T. C. Bailey, B. J. Choi, M. Colburn, M. Meissl, S. Shaya, J. G. Ekerdt, S. V. Sreenivasan, C. G. Willson, *J. Vac. Sci. Technol. B* **2000**, 18, 3572.
- [8] T. C. Bailey, S. C. Johnson, S. V. Sreenivasan, J. G. Ekerdt, C. G. Willson, D. J. Resnick, *J. Photopolym. Sci. Technol.* **2002**, 15, 481.
- [9] D. J. Resnick, W. J. Dauksher, D. Mancini, K. J. Nordquist, T. C. Bailey, S. Johnson, N. Stacey, J. G. Ekerdt, C. G. Willson, S. V. Sreenivasan, N. Schumaker, *J. Vac. Sci. Technol. B* **2003**, 21, 2624.
- [10] G. Y. Jung, S. Ganapathiappan, D. A. A. Ohlberg, D. L. Olynick, Y. Chen, W. M. Tong, R. S. Williams, *Nano Lett.* **2004**, 4, 1225.
- [11] M. D. Stewart, C. G. Willson, *MRS Bulletin* **2005**, 30, 947.
- [12] B. K. Long, B. K. Keitz, C. G. Willson, *J. Mater. Chem.* **2007**, 17, 3575.

- [13] G. Y. Jung, E. Johnston-Halperin, W. Wu, Z. N. Yu, S. Y. Wang, W. M. Tong, Z. Y. Li, J. E. Green, B. A. Sheriff, A. Boukai, Y. Bunimovich, J. R. Heath, R. S. Williams, *Nano Lett.* **2006**, *6*, 351.
- [14] L. J. Guo, *J. Phys. D: Appl. Phys.* **2004**, *37*, R123.
- [15] L. J. Guo, *Adv. Mater.* **2007**, *19*, 1.
- [16] T. Leveder, S. Landis, L. Davoust, N. Chaix, *Microelect. Engin.* **2007**, *84*, 953.
- [17] Y. Ding, H. W. Ro, J. F. Douglas, R. L. Jones, D. R. Hines, A. Karim, C. L. Soles, *Adv. Matter.* **2007**, *19*, 1377.
- [18] a) G. L. W. Cross, *J. Phys. D: Appl. Phys.* **2006**, *39*, R363. b) G. L. W. Cross, B. S. O'Connell, J. B. Pethica, *Appl. Phys. Lett.* **2005**, *86*, 081902.
- [19] K. Y. Suh, P. Kim, H. H. Lee, *Appl. Phys. Lett.* **2004**, *85*, 4019.
- [20] Y. Hirai, S. Yoshida, N. Takagi, Y. Tanaka, H. Yabe, K. Sasaki, H. Sumitani, K. Yamamoto, *Jap. J. Appl. Phys.* **2003**, *42*, 3863.
- [21] W. W. Mullins, *J. Appl. Phys.* **1957**, *28*, 333; **1959**, *30*, 77.
- [22] M. Hamdorf, D. Johannsmann, *J. Chem. Phys.* **2000**, *112*, 4262.
- [23] E. Buck, K. Petersen, M. Hund, G. Krausch, D. Johannsmann, *Macromolecules* **2004**, *37*, 8647.
- [24] G. T. Dee, B. B. Sauer, *Adv. Phys.* **1998**, *47*, 161.
- [25] J. D. Ferry, *Viscoelastic Properties of Polymers*, 3rd edn, John Wiley & Sons, New York **1980**.
- [26] J. C. Majeste, J. P. Montfort, A. Allal, G. Marin, G. *Rheol. Acta.* **1998**, *37*, 486.
- [27] E. B. Bagley, D. C. West, *J. Appl. Phys.* **1958**, *29*, 1511.
- [28] R. S. Porter, J. F. Johnson, *J. Appl. Phys.* **1961**, *32*, 2326.
- [29] L. Ressler, C. Martin, J. P. Peyrade, *Microelect. Engin.* **2004**, *71*, 272.
- [30] F. Kremer, A. Schönhal, *Broadband dielectric spectroscopy*, Springer, New York, **2003**.
- [31] H. Schulz, M. Wissen, N. Bogdanski, H. C. Scheer, K. Mattes, C. Friedrich, *Microelect. Eng.* **2006**, *83*, 259.
- [32] H. Schulz, M. Wissen, N. Bogdanski, H. C. Scheer, K. Mattes, C. Friedrich, *Microelect. Eng.* **2005**, *78–79*, 625.
- [33] K. J. Alvine, H. W. Ro, Y. Ding, J. F. Douglas, B. C. Okerberg, K. A. Lavery, W. E. Wallace, S. Lin-Gibson, A. Karim, C. L. Soles, Unpublished.
- [34] Z. Li, M. Tolan, T. Höhr, D. Kharas, S. Qu, J. Sokolov, M. H. Rafailovich, H. Lorenz, J. P. Kotthaus, J. Wang, S. K. Sinha, A. Gibaud, *Macromolecules* **1998**, *31*, 1915.
- [35] Z. N. Yu, L. Chen, W. Wu, H. X. Ge, S. Y. Chou, *J. Vac. Sci. Tech. B* **2003**, *21*, 2089.
- [36] G. Y. Jung, Z. Li, W. Wu, Y. Chen, D. L. Olynick, S. Y. Wang, W. M. Tong, R. S. Williams, *Langmuir* **2005**, *21*, 1158.
- [37] R. L. Jones, T. Hu, E. K. Lin, W. L. Wu, R. Kolb, D. M. Casa, P. J. Bolton, G. G. Barclay, *Appl. Phys. Lett.* **2003**, *83*, 4059.
- [38] T. J. Hu, R. L. Jones, W. L. Wu, E. K. Lin, Q. H. Lin, D. Keane, S. Weigand, J. Quintana, *J. Appl. Phys.* **2004**, *96*, 1983.
- [39] R. L. Jones, T. J. Hu, C. L. Soles, E. K. Lin, W. Hu, R. M. Reano, S. W. Pang, D. M. Casa, *J. Microlith, Microfab, Microsyst.* **2005**, *5*, 013001.
- [40] H. J. Lee, C. L. Soles, H. W. Ro, R. L. Jones, E. K. Lin, W. L. Wu, D. R. Hines, *Appl. Phys. Lett.* **2005**, *87*, 263111.
- [41] H. J. Lee, H. W. Ro, C. L. Soles, R. L. Jones, E. K. Lin, W. L. Wu, D. R. Hines, *J. Vac. Sci. Tech. B* **2005**, *23*, 3023.
- [42] Y. Ding, H. W. Ro, T. A. Germer, J. F. Douglas, B. C. Okerberg, A. Karim, C. L. Soles, *ACS Nano* **2007**, *1*, 84.